THE ASTROPHYSICAL JOURNAL, 366:484–494, 1991 January 10

A DETAILED OPTICAL STUDY OF KEPLER'S SUPERNOVA REMNANT

WILLIAM P. BLAIR,[1] KNOX S. LONG,[1,2] AND OLAF VANCURA
Department of Physics and Astronomy, Johns Hopkins University
Received 1990 May 4; accepted 1990 July 5

ABSTRACT

We present optical CCD/interference filter imagery and long-slit CCD spectrophotometry of the remnant of Kepler's supernova (SN 1604 A.D.) obtained with the 2.5 m DuPont telescope at the Las Campanas Observatory. Subtraction of a continuum image from the emission line image shows the full extent of the optical emission of the supernova remnant, which has both diffuse and knotty structures. Spectroscopy in the 4700–7000 Å range confirms the presence of nonradiative, Balmer-dominated, shock emission in Kepler's remnant and shows this emission to be much more extensive than previously realized, extending to knotty structures as well as diffuse emission. This is the first report of nonradiative shock emission from filaments with a knotty morphology. Emission knots are also identified which appear to be at intermediate stages of becoming radiative. The shock velocity in the Balmer-dominated shocks is 1530–2000 km s^{-1}. If this is the expansion velocity of the entire supernova remnant, the distance to Kepler's SNR is 2.9 ± 0.4 kpc.

Subject headings: nebulae: individual (Kepler's supernova) — nebulae: internal motions — nebulae: supernova remnants — radiation mechanisms

I. INTRODUCTION

Because of its prominence as one of only a handful of historical supernova remnants (SNRs), the remnant of SN 1604 A.D. (often called Kepler's SNR) has received considerable attention by observers at many wavelengths. Baade (1943) first identified the optical SNR as a few faint knots of emission on red plates taken with the 100″ telescope at Mount Wilson. van den Bergh and Kamper (1977) studied brightness variations and proper motions of the filaments photographically, concluding that the optical emission was largely circumstellar material from the precursor now being excited by interaction with the SN blast wave. In contrast, the X-ray and radio emissions from the remnant show a circular, limb-brightened, nearly complete ring of emission with diameter ~200″ and brightest on the northern rim (White and Long 1983; Hughes and Helfand 1985; Matsui *et al.* 1984; Dickel *et al.* 1988). Kepler's SNR has an IR luminosity in excess of its soft (0.2–4 keV) X-ray luminosity, although it is too small to have been well-resolved by *IRAS* (Dwek *et al.* 1987; Braun 1987). The X-ray and radio emissions presumably show the true extent of the blast wave. Comparison with optical photographs shows that the brightest optical filaments coincide with the western and northwestern portions of the SNR shell.

Optical spectra of the bright knots in Kepler's SNR (Dennefeld 1982; Leibowitz and Danziger 1983) confirm that these filaments are due to radiative shock waves, although with several peculiarities. From the observed [S II] λλ6717:6731 line ratios, it appears that the optical filaments have fairly high densities ($n_e \geq 1000$ cm^{-3}) compared with many other galactic SNRs. The extinction is reported to be quite high and variable from filament to filament (Leibowitz and Danziger 1983). Lastly, these filaments show very strong [N II] λλ6584, 6548 emission relative to Hα. The observed emission corresponds to a factor of ~3.5 enhancement in *N* abundance over solar, much too large to be attributed to a Galactic abundance gradient effect (see Fesen, Blair, and Kirshner 1985). This presumably points to a circumstellar origin of the optically emitting gas, which is somewhat at odds with the identification of the SN as a Type Ia and the current theory of the origin of such SNs in low-mass stars (Nomoto, Thielemann, and Yokoi 1984), and has led to suggestions that Kepler's SN was actually of Type Ib (Bandiera 1987).

The distance to Kepler's SNR is not well-known, with published estimates ranging from 3–12 kpc (see summary in Green 1984). Since these distance estimates rely on such parameters as the Hubble constant, the observed apparent magnitude and color of the supernova, and radio surface brightness-diameter correlations, the spread of distance estimates is understandable. Kepler's SNR is located well off the Galactic plane ($b^{II} = 6.°8$; only three Galactic SNRs have higher latitudes – see van den Bergh 1978), so distance estimates using optical extinction or N_H column densities only provide consistency checks. A distance of 5 kpc is consistent with most of the available data and obviates the need for rather high mean expansion velocities at the larger distances. At 5 kpc, Kepler's SNR has a *z* distance of 600 pc, a diameter of 3.8 pc, and a mean expansion velocity of ~5000 km s^{-1}.

Recently, additional optical emission was identified in Kepler's SNR by D'Odorico *et al.* (1986) using a CCD with an Hα + [N II] interference filter. Although these authors concentrated on cataloging the newly detected knots, considerable diffuse emission is also visible in their images. Fesen *et al.* (1989) obtained images and spectra of some of the diffuse emission in the north and found it to be dominated by hydrogen Balmer emission. Careful inspection of the line widths at Hα showed the line to have both broad and narrow components, indicating nonradiative shocks in Kepler's SNR (see Chevalier, Kirshner, and Raymond 1980, hereafter CKR). Such emission indicates a fast shock wave encountering partially neutral preshock material. These shocks are termed nonradiative because the radiative or recombination time scale behind the shock is long in comparison with the dynamical timescale. This type of emission has been seen as crisp filaments at the periphery of

[1] Visiting Astronomer, Las Campanas Observatory, operated by the Carnegie Institution of Washington.
[2] Visiting Adjunct Associate, Mount Wilson and Las Campanas Observatories.

several SNRs, including Tycho's SNR, SN 1006 and on the outskirts of the Cygnus Loop in our Galaxy (Long, Blair, and van den Bergh 1988; Kirshner, Winkler, and Chevalier 1987; Raymond *et al.* 1983), and several Large Magellanic Cloud SNRs (Tuohy *et al.* 1982). The nonradiative emission found by Fesen *et al.* (1989) in Kepler's SNR has a distinctly diffuse appearance, although it is located at the northern periphery.

In this paper, we report extensive imagery and spectroscopy of Kepler's SNR and identify considerably more nonradiative emission. The imaging observations are described in § II, followed by the spectroscopy in § III, and a discussion in § IV.

II. IMAGERY

A preliminary report of our imagery was given in Fesen *et al.* (1989), although only the Hα + [N II] image was shown there. We used a TI 800 × 800 CCD with a focal reducer on the 2.5 m DuPont telescope at Las Campanas Observatory to obtain images of Kepler's SNR in 1987 April. The focal reducer (the CHUEI – similar to the PFUEI described by Gunn and Westphal 1981) compressed the f/7.5 telescope beam down to f/2.7, yielding a scale of 0.″41 pixel^{-1} on the CCD and providing a field 5.′3 square. The following interference filters and exposure times were used: an Hα filter (λ_0 = 6565 Å, FWHM = 30 Å; 2000 s), a [S II] filter (λ_0 = 6737 Å, FWHM = 57 Å; 4000 s), an [O I] filter (λ_0 = 6300 Å, FWHM = 50 Å; 4000 s), a red continuum filter (λ_0 = 6100 Å, FWHM = 130 Å; 2000 s), and an [O III] filter (λ_0 = 5027 Å, FWHM = 53 Å; 4000 s). The seeing was 1.″0 ± 0.″1 (FWHM) for all images and transparency was excellent. Spectrophotometric standard stars were observed through the filters each night.

The CCD images were bias-subtracted and divided by normalized flat fields to take out pixel-to-pixel variations in the CCD. Also, because much of the emission is knotty or nearly stellar in appearance and exceedingly faint, sky background was subtracted and the continuum image was aligned, scaled, and subtracted from each emission-line image to remove the stars (to first-order). Figure 1 (Plate 10) shows a 600 × 650 pixel region of the reduced Hα image before sky and continuum subtraction, highlighting the brighter knots for comparison with previously published photographs. Figure 2 (Plates 11–14) shows all of the emission-line images after alignment and continuum subtraction, stretched to highlight the faintest detected emission.

The most dramatic result was obtained with the Hα filter. This filter was broad enough that the [N II] lines could enter in the far wings of the filter transmission, especially λ6583, which is stronger than Hα in Kepler's radiative filaments. The subtracted Hα image (Fig. 2*a*) shows all of the knots reported by D'Odorico *et al.* (1986), as well as additional knots and faint diffuse emission surrounding and interconnecting many of the knots. Some of the fainter knots are not detected in the other emission-line images, and the diffuse emission also appears to be absent. This can be seen clearly in Figure 3 (Plate 15), which shows the ratio of subtracted Hα and [S II] images from Figure 2. Since [N II] and [S II] emission in radiative shocks usually track one another quite well, the implication is that the emission showing as black in Figure 3 is dominated by Hα emission.

Comparisons of the optical images with the X-ray (Fig. 4, [Pl. 16]) and radio (Fig. 5, [Pl. 17]) maps of Kepler are interesting. The reprocessed *Einstein* X-ray data were kindly provided by Fred Seward (1989, private communication; see also Seward 1990) and show the 0.2–4 keV emission from the remnant. The radio image is 6 cm data from the VLA as published by Matsui *et al.* (1984). The images have been aligned using the radio data and the optical astrometry of D'Odorico *et al.* (1986). The X-ray and radio morphologies of Kepler's SNR are quite similar, as has been noted previously (see Strom 1988). The similarity between the X-ray and radio map has been used to align the X-ray data to the radio data because the nominal X-ray coordinates appeared shifted by ~10″ to the southeast. In both wavelength ranges a bright shell which can be traced over $\frac{3}{4}$ of the periphery of the remnant dominates the appearance of the SNR. There is also a ridge of emission which crosses the center of the SNR. Emission is weakest in the southwest at all wavelengths, which presumably is indicative of lower densities there. Bandiera (1987) has argued that this density gradient is due to the interaction of the stellar wind of the progenitor with the ISM as the pre–SN star moved through the ambient gas. Bright radiative optical filaments in Kepler's SNR, as evidenced by our forbidden line images and previous optical studies, are found mainly on the NW edge of the SNR; this is the brightest portion of the X-ray shell as well, although the correspondence between the brightest optical and X-ray emission is not particularly striking. Radio emission is brightest along the northern edge of the SNR. If one considers the fainter optical emissions, those which are seen predominantly as Hα-dominated filaments, there is a better correspondence between features seen in the optical and at other wavelengths. The faint Hα-dominated filaments in the north are located on the outside edge of the radio and X-ray shell. The displacement between the peak Hα and the radio or X-ray emission is about 15″. This suggests that the X-ray/radio shell is thicker than the shell associated with optical Hα emission or, alternatively, that there is a delay between the passage of the shock and the onset of copious X-ray/radio emission. The former seems much more likely, since the Hα ionization time scale is very short. The clusters of faint optical knots near the center of the remnant show a general correspondence with enhancements in the X-ray and/or radio maps which has not been recognized before.

III. SPECTROPHOTOMETRY

In order to elucidate the character of the emission in many of the fainter emission regions in Kepler's SNR, we have obtained long-slit CCD spectra at the four positions indicated in Figure 1. These spectra were taken in 1988 August and 1989 August with a CCD spectrograph on the 2.5 m DuPont telescope at Las Campanas Observatory. The 1988 data were obtained with a 600 line mm^{-1} 5000 Å blaze grating and a 2.″5 slit width yielding spectra from 4700–7150 Å with ~8 Å resolution. The 1989 spectra were taken with a 1200 line mm^{-1} 7500 Å blaze grating centered at Hα and a 2″ slit width which yielded ~3.5 Å resolution over the 6100–7250 Å range. The higher resolution observations are particularly important because they reveal information about the shape of the Hα line in nonradiative filaments. The spatial scale provided by the "fast" camera (85 mm f/1.2) was 0.″85 pixel^{-1} and the useful slit length was ~7′. The spectrograph could be rotated on the back of the telescope to place the long slit so as to maximize the number of knots observed. A different rotation angle was chosen for position 3 in the higher resolution data, resulting in position 3*a* in Figure 1. These observations are summarized in Table 1.

These spectra have been reduced at Johns Hopkins using IRAF. Each two-dimensional spectrum was background-

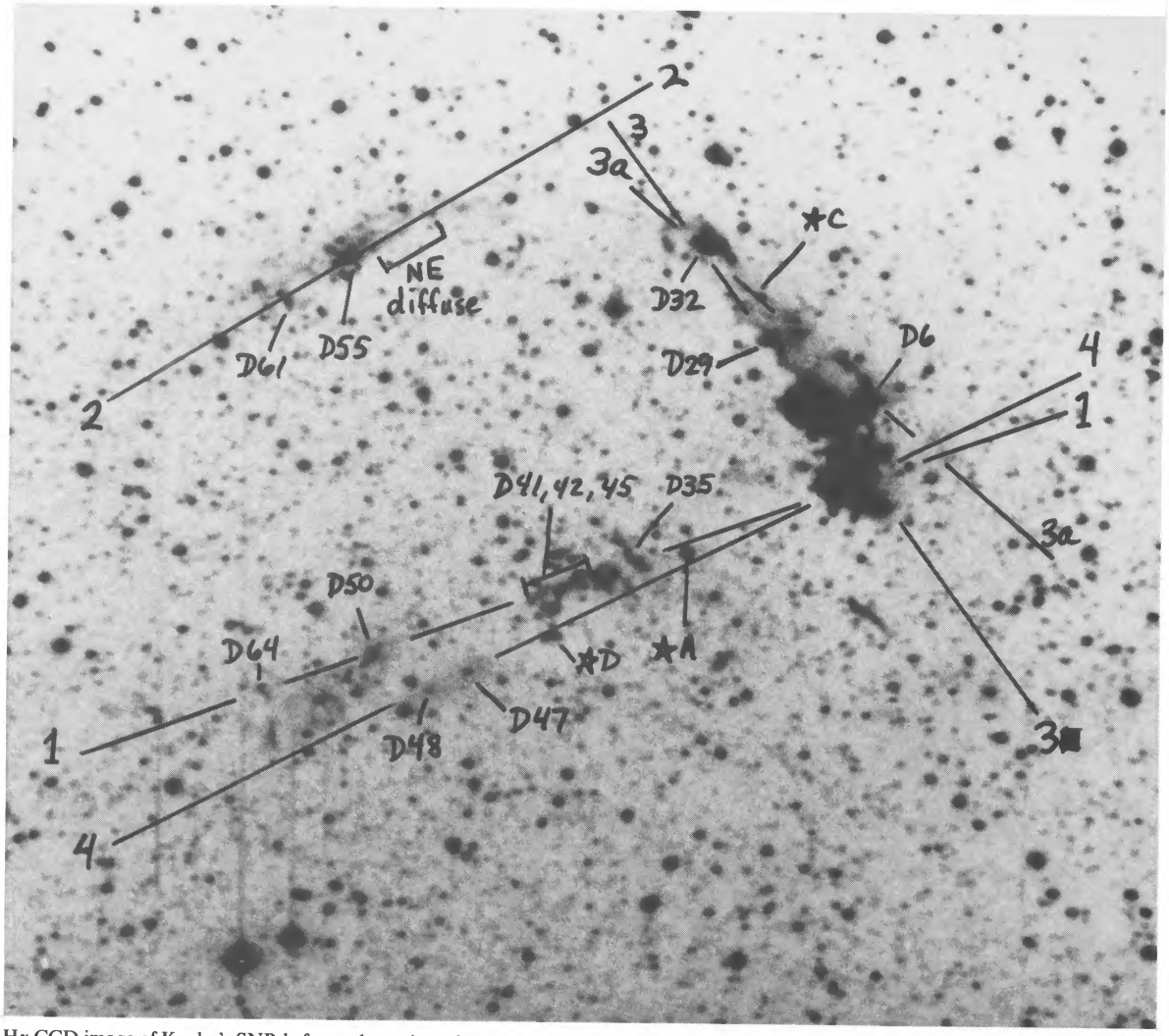

FIG. 1.—Hα CCD image of Kepler's SNR before subtraction of stellar contamination. The field shown is 4.'1 vertically and 4.'4 horizontally. Slit positions for our long-slit spectra are indicated along with some fiducial stars. North is up and east is to the left.

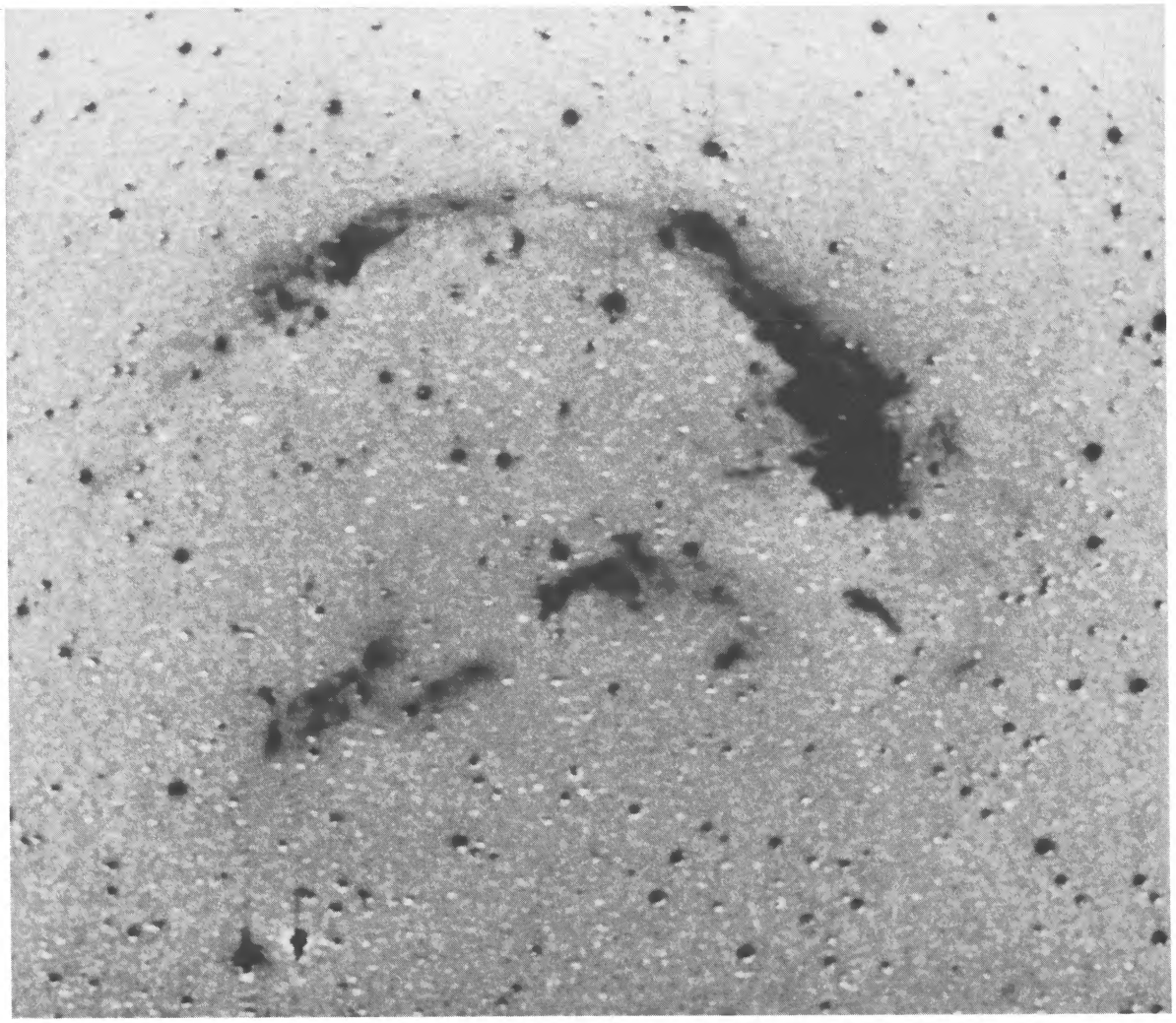

FIG. 2*a*

FIG. 2.—Continuum-subtracted emission line CCD images of Kepler's SNR. Scale and orientation are the same as in Figure 1. (*a*) Hα; (*b*) [S II]; (*c*) [O I]; (*d*) [O III]. For various reasons, the stellar subtractions of the Hα images left fewer stellar residuals than the other emission-line images. Note, however, that some of the faint Hα emission knots in the central, NE, and NW portions of the remnant remain visible on some or all of the other images, while the diffuse emission and many of the fainter knots disappear.

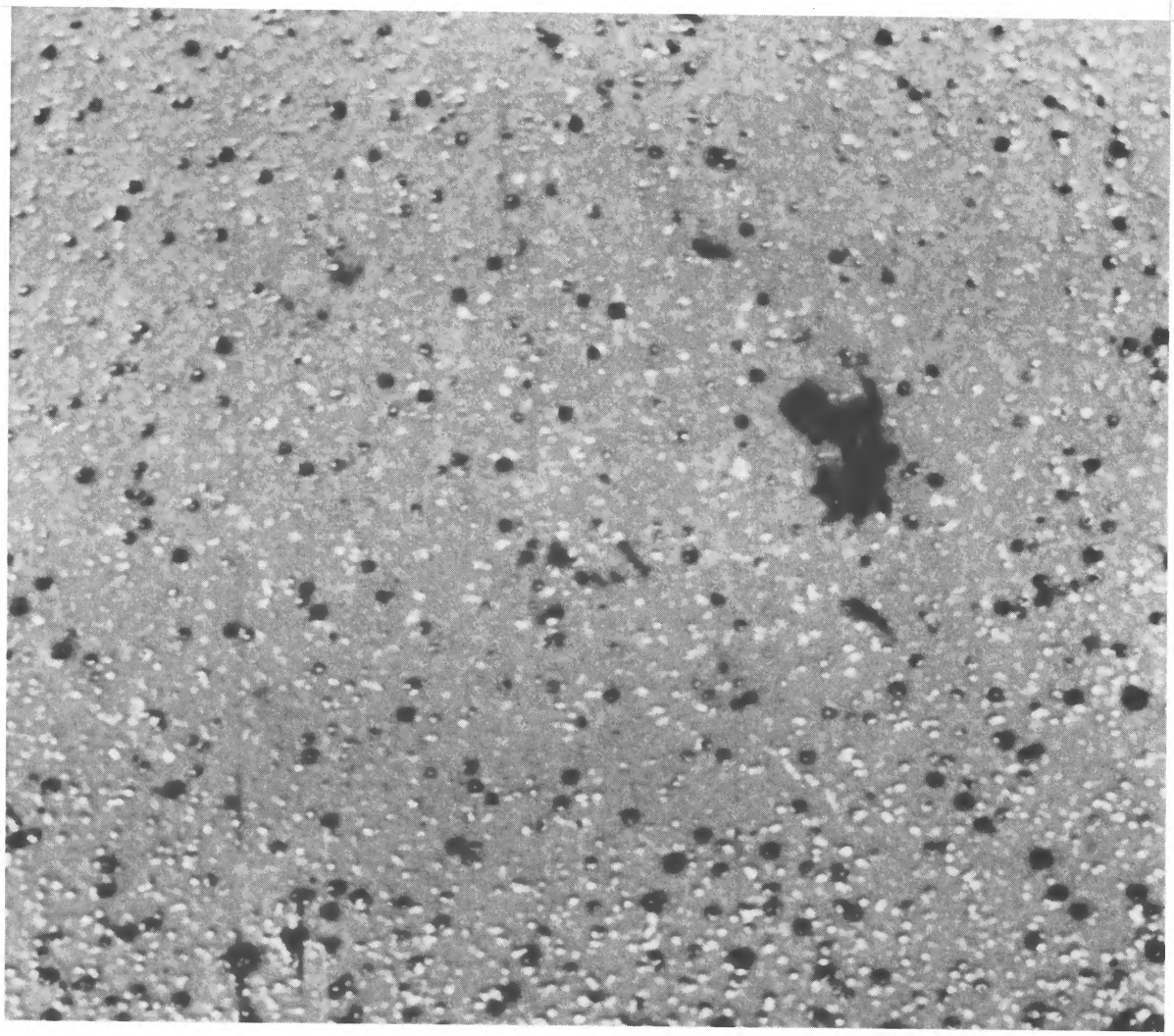

FIG. 2*b*

BLAIR, LONG, AND VANCURA (*see* **366**, 485)

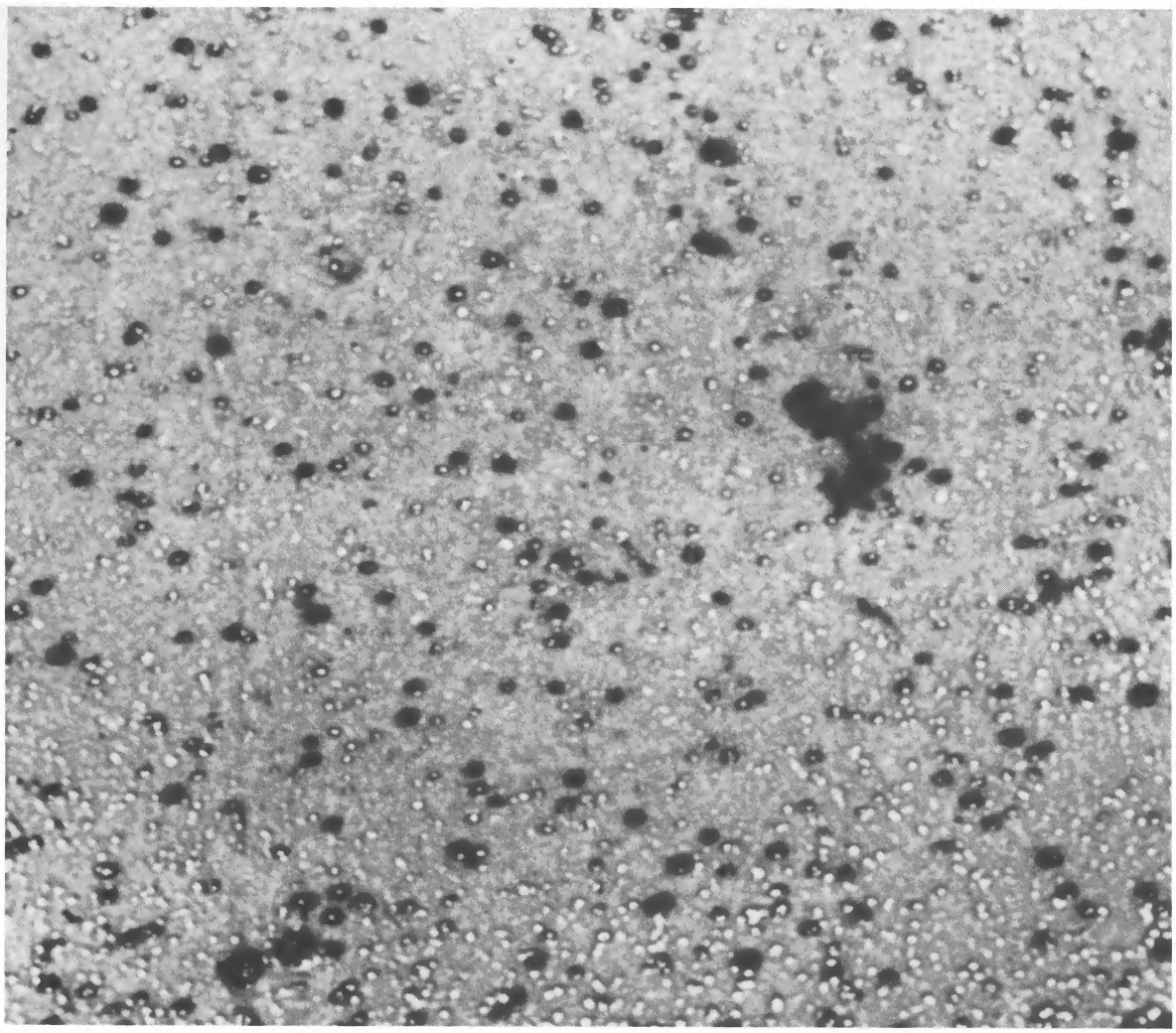

FIG. 2*c*

BLAIR, LONG, AND VANCURA (*see* **366**, 485)

PLATE 14

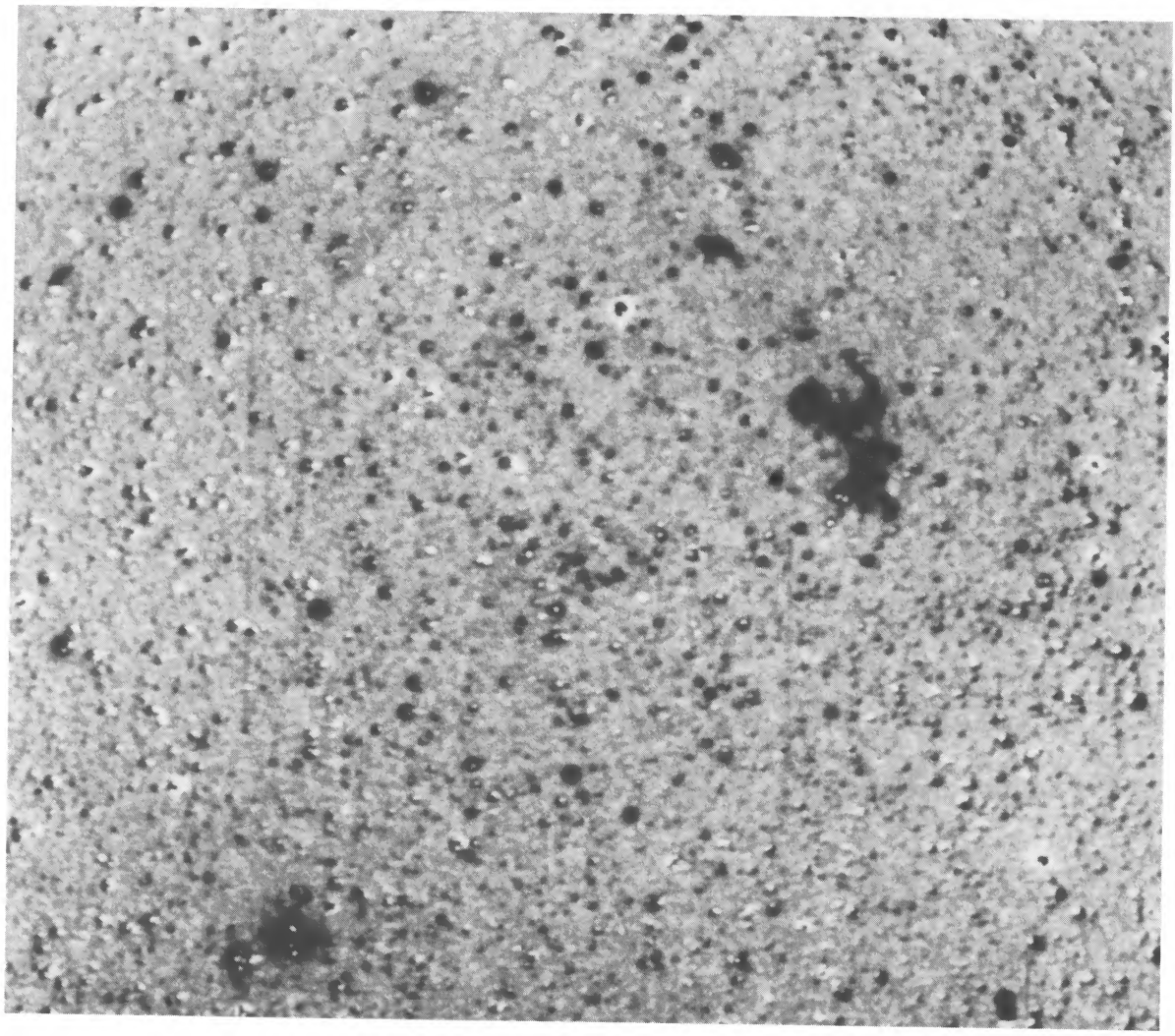

FIG. 2*d*

FIG. 3.—Ratio map of the subtracted Hα and [S II] images from Figure 2. Knots showing on both images appear white (as do stellar residuals) while emission dominated by Hα remains black.

PLATE 16

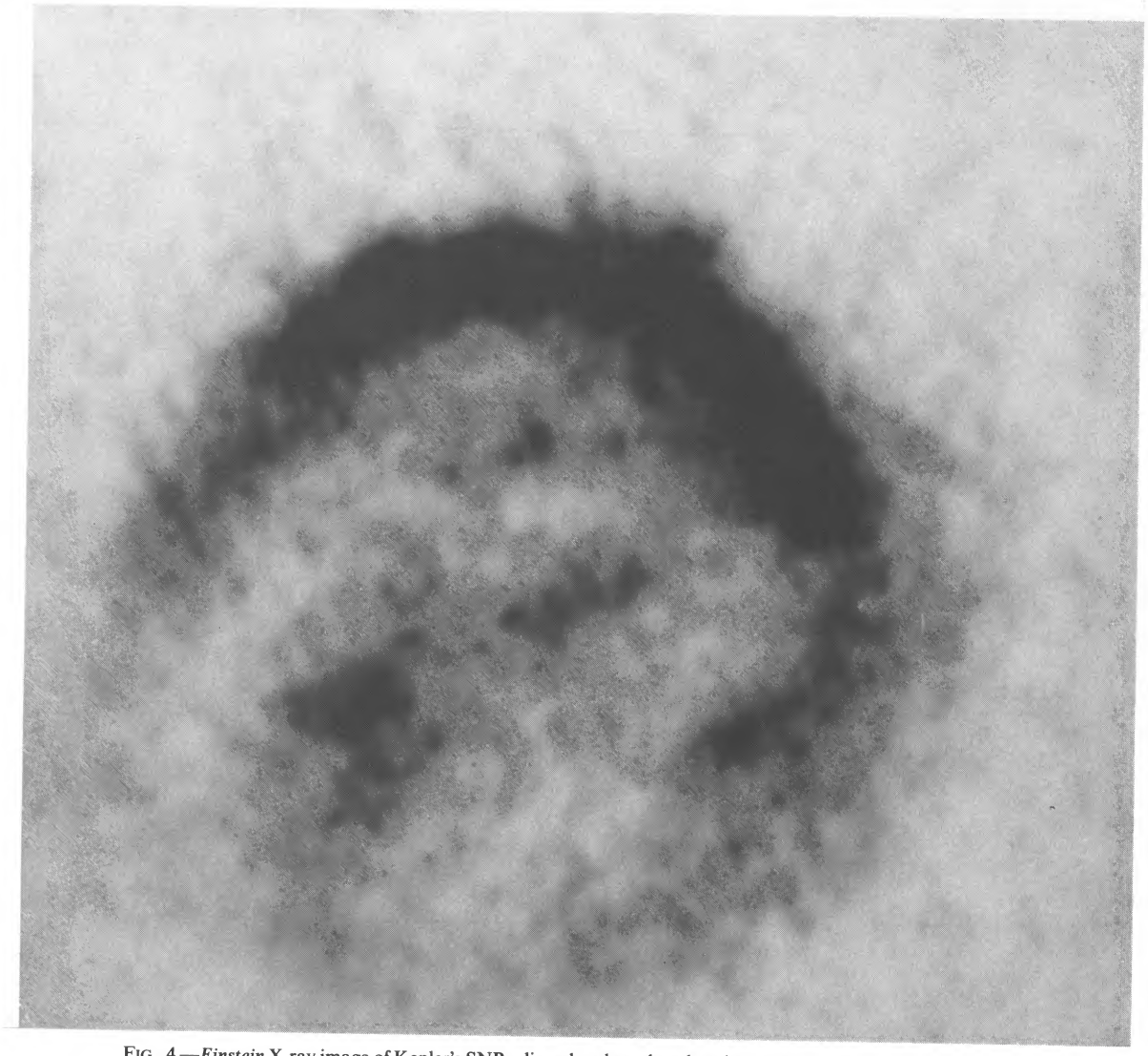

FIG. 4.—*Einstein* X-ray image of Kepler's SNR, aligned and produced to the same scale as Figures 1 and 3

BLAIR, LONG, AND VANCURA (*see* **366**, 485)

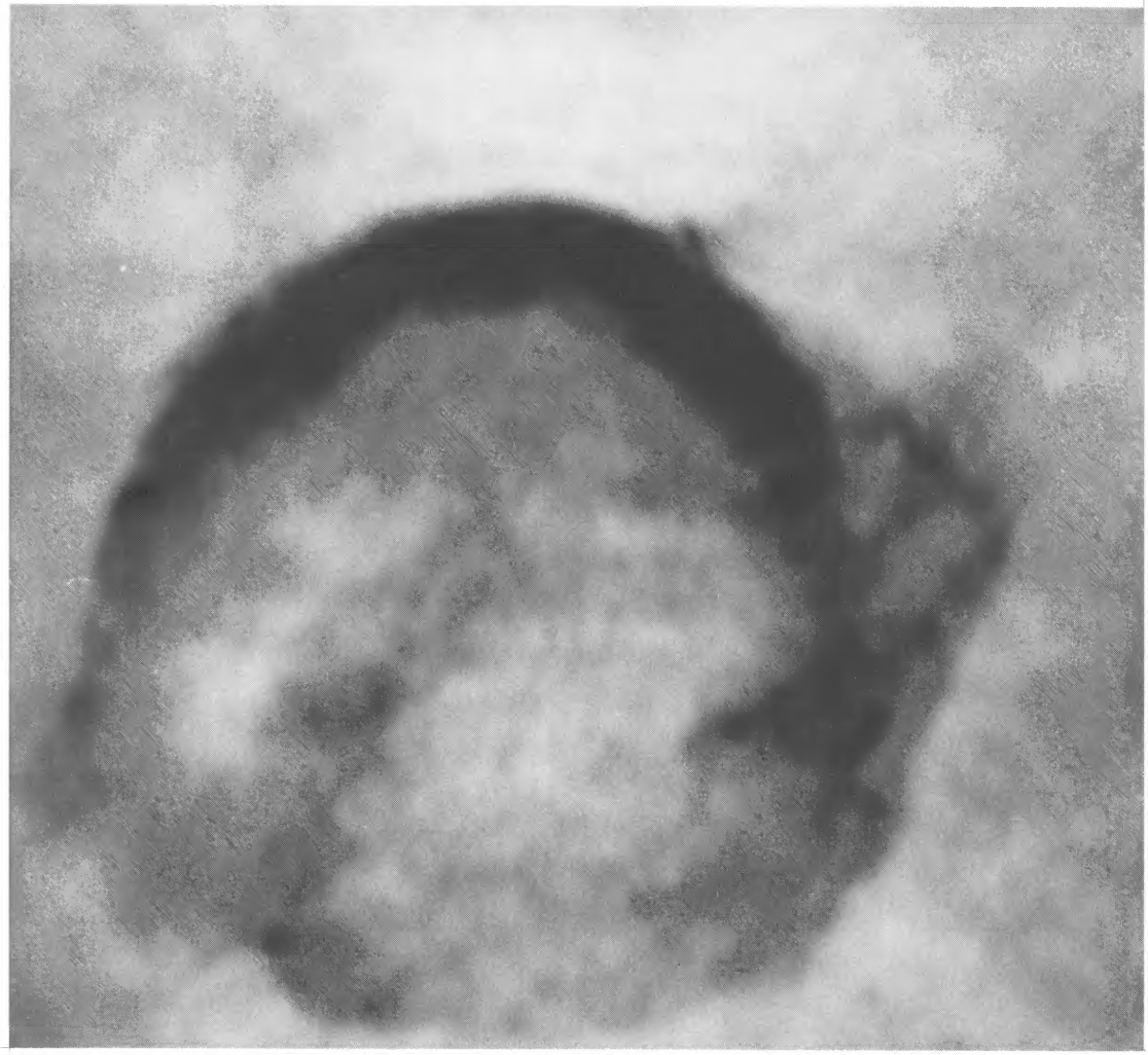

FIG. 5.—The 6 cm VLA radio map of Kepler's SNR (data from Matsui *et al.* 1984) produced to the same scale as Figures 3 and 4

TABLE 1

SPECTROPHOTOMETRIC OBSERVATIONS OF KEPLER'S SNR

Position	Date (UT)	Instrument Configuration[a]	Integration(s)	Position Angle	Condition
P1	1988 Aug 17	1	2400	110°	lt. cirrus
	1989 Aug 26	2	2 × 3600	110	lt. cirrus
P2	1988 Aug 17	1	2400	120	clear
	1989 Aug 26	2	4200	120	lt. cirrus
P3	1988 Aug 20	1	1800	38	clear
P3*a*	1989 Aug 27	2	6000	52	clear
P4	1988 Aug 20	1	3600	116	clear
	1989 Aug 27	2	3600	120	clear

[a] Configuration No. 1 is 4700–7000 Å coverage with 8 Å resolution; configuration No. 2 is 6100–7250 Å with 3.5 Å resolution.

subtracted, flat-fielded, wavelength-calibrated, and transformed to remove instrumental distortions. The flux calibration was applied using observations of spectrophotometric standard stars from Stone and Baldwin (1983). This removed the effects of the instrumental response and placed the observed line intensities on the proper relative scale. A comparison of the standard stars EG 274, LTT 7379, and LTT 1020 indicates the absolute fluxes are accurate to $\sim 30\%$ for both the high- and low-resolution spectra. It also indicates an uncertainty in relative calibration of the blue and red end of the low-resolution spectra of $\leq 10\%$.

Figure 6 (Plate 18) shows the Hα and [N II] regions from the four high-resolution spectral positions in two-dimensional format. Vertical lines are due to the night sky and horizontal lines are stars whose light entered the slit. Several stars that were used as fiducials are indicated with letters on Figure 6 and Figure 1. The labels along the spatial dimension of Figure 6 correspond to knot numbers from the list of D'Odorico *et al.* (1986) and are used as well in Table 2 and Figure 1. As seen previously, the bright radiative filaments in the NW are dominated by very strong [N II] and [S II] forbidden line emission. However, many of the faint knots and regions of diffuse emission are dominated by hydrogen Balmer emission (see also Fig. 3). In the most extreme cases observed (e.g., D47, D48, D50) there is no discernible [S II] or [N II] emission, while in other cases (D61, D41, D42) the [N II] or [S II] lines are seen but are weaker than Hα, in contrast with the bright NW filaments. Some of the fainter knots (e.g., D64) also show strong [S II] and [N II] lines relative to Hα, similar to the brighter radiative filaments. Careful inspection of these data make it clear that, in the cases with weaker than normal forbidden line emission, the spatial extent of the forbidden lines is consistent with that of Hα. This makes it clear that the forbidden line emission is not due to normal radiative emission seen in projection against Balmer filaments, but is probably due to a "transition" between these two types.

One-dimensional spectra representing each knot or region of diffuse emission have been extracted from the two-dimensional data using the "apextract" package in IRAF. Regions for sky subtraction were chosen carefully from adjacent regions along the slit that do not show any SNR emission. Figure 7 shows a montage of representative low-resolution spectra that have been extracted in this fashion. The line intensities of these and other spectra have been measured and are tabulated in Table 2 on a scale where Hα = 300; the measured and corrected Hα fluxes for each knot are shown at the bottom of each column. In those knots where Hβ was accurately measured, we also show reddening-corrected line intensities (assuming a Seaton 1979 curve and an intrinsic Hα:Hβ ratio of 3.0) and the derived value of $E(B-V)$. For those knots where Hβ could not be measured accurately, the mean extinction from the brighter knots has been assumed [$E(B-V) = 0.90$].

Similarly, Figure 8 shows the range of Hα line shapes we have observed with the higher resolution setup on the modular spectrograph. Knot D3 shown in Figure 8*a* is a typical radiative filament in the SNR. The spectra of knots D49 and D50 (Fig. 8*b*) and of D47 and D48 (Fig. 8*c*) are typical of the cleanest Balmer-dominated filaments. There is little if any [N II] emission and the Hα line profile clearly has a broad component. The spectrum of knots D41, D42, D44, and D45 (Fig. 8*d*) shows not only evidence of a broad component to the Hα line profile expected in a nonradiative filament but also of narrow [N II] emission expected from a radiative filament.

In order to characterize the shapes of the Hα profiles in the nonradiative filaments we have fit the spectra to various models which can have as many as five components—broad and narrow Hα, [N II] λ6548, [N II] λ6583, and a linear background term. For this analysis we have used a χ^2 minimizing line-fitting program, "specfit," kindly provided to us by G. A. Kriss, which provides a convenient method for fixing and/or freeing various parameters involved in the model fits. Results of the model fits for the four cleanest nonradiative spectra, as well as several radiative spectra are presented in Table 3. We considered three possibilities for modeling the filaments: (I) broad and narrow Hα without the [N II] lines; (II) narrow Hα and the [N II] lines with no broad component; and (III) broad and narrow Hα in addition to the [N II] lines. Errors (1 σ) are given for those parameters which were allowed to vary. Usually there are three parameters for each line, the line center, the line width and the line strength, which are allowed to vary. However, we fixed the widths of the [N II] lines to equal those in a clean radiative filament spectrum since any broad [N II] emission would be too weak to be observed.

The average FWHM of the broad component in the four cleanest examples is ~ 34 Å or ~ 1550 km s^{-1}. This value is slightly lower than (but consistent with) the value found for the diffuse emission in the north by Fesen *et al.* (1989). The ratio of flux in the broad and narrow components is 0.72 ± 0.37, also somewhat lower than the value of 1.1 ± 0.25 found by Fesen *et al.* (1989). The new values should probably be preferred because we have sampled more filaments and because our spectra have improved resolution.

PLATE 18

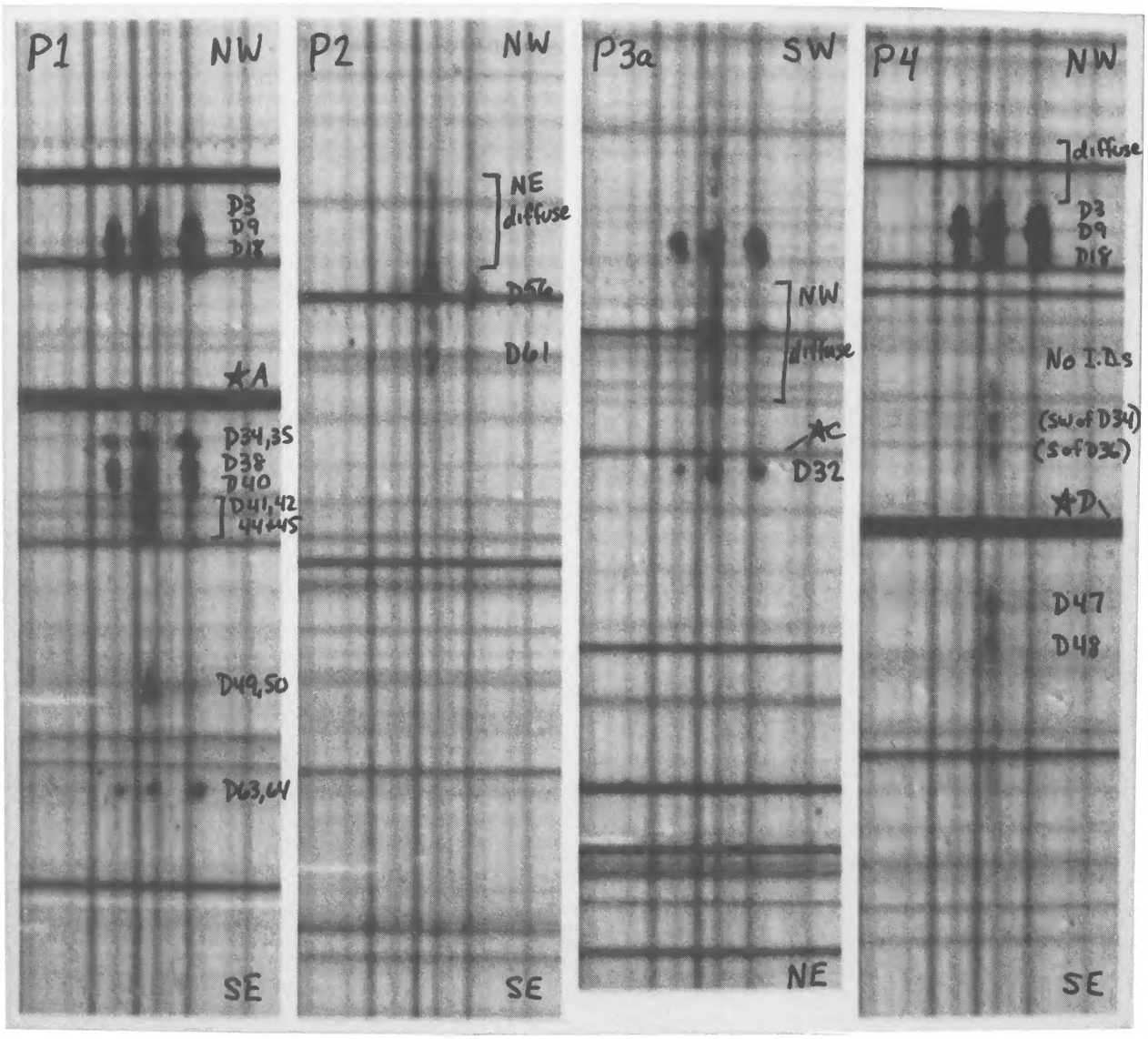

FIG. 6.—Two-dimensional long-slit spectra of slit positions (*a*) P1, (*b*) P2, (*c*) P3*a*, and (*d*) P4. Here the Hα-[N II] region of each spectrum has been extracted to show the spatial slit profiles and variation of Hα and [N II] line strengths. Letters identify fiducial stars from Figure 1, and numbers identify knots catalogued by D'Odorico *et al.* (1986).

TABLE 2

OBSERVED $F(\lambda)$ AND CORRECTED $I(\lambda)$ LINE INTENSITIES IN KEPLER'S SNR FROM LOW-DISPERSION SPECTRA

		KNOT IDENTIFICATION[a]									
		D3[b]		D9[b]		D18[b]		D34, 35		D38, 40	
LINE	λ	$F(\lambda)$	$I(\lambda)$	$F(\lambda)$	$I(\lambda)$	$F(\lambda)$	$I(\lambda)$	$F(\lambda)$	$I(\lambda)$	$F(\lambda)$	$I(\lambda)$
Hβ	4861	37.5	100.0	41.5	100.0	34.8	100.0	...	...	37.1	100.0
[O III]	4959	28.0	69.5	19.6	44.3	12.2	32.5	...	...	21.2	53.2
[O III]	5007	92.0	222.3	62.3	137.3	33.3	86.1	...	...	67.1	163.7
[N II]	5755	14.7	21.9	12.7	18.2	12.2	18.8	...	...	9.9	14.8
He I	5876	13.6	18.9	8.7	11.6	15.2:	21.5:	10.8:	15.0:	5.8	8.1
[O I]	6300	51.1	57.4	69.2	76.8	170.4	192.8	90.0	101.0	49.4	55.5
[O I]	6363	20.1	21.9	21.9	23.7	59.3	65.0	34.8	38.0	16.4	17.9
[N II]	6548	146.6	147.5	150.0	150.8	222.2	223.6	132.0	132.8	95.3	95.9
Hα	6562	300.0	300.0	300.0	300.0	300.0	300.0	300.0	300.0	300.0	300.0
[N II]	6583	443.2	439.3	461.5	457.9	703.7	697.0	378.0	374.7	282.4	279.8
[S II]	6717	102.3	96.1	70.4	66.6	137.0	128.2	42.0	39.5	21.2	19.9
[S II]	6731	170.5	159.4	138.5	130.4	274.1	255.0	84.0	78.5	40.6	37.9
F(Hα), I(Hα)[c]		8.8	69.0	26.0	164.4	8.1	74.2	5.0	39.5	17.0	136.6
N_e (cm^{-3})		2200		4900		5400		5400		4000	
$E(B-V)$[d]		0.8969		0.8034		0.9648		0.9005[e]		0.9077	

		KNOT IDENTIFICATION[a]									
		D49, 50		D63, 64		D41–45		D55		D56	
LINE	λ	$F(\lambda)$	$I(\lambda)$	$F(\lambda)$	$I(\lambda)$	$F(\lambda)$	$I(\lambda)$	$F(\lambda)$	$I(\lambda)$	$F(\lambda)$	$I(\lambda)$
Hβ	4861	...	...	...	...	40.9	109.5	37.7	100.0	...	...
[O III]	4959	...	...	...	...	...	...	...	...	...	...
[O III]	5007	...	...	...	...	...	...	7.0	16.8	...	...
[N II]	5755	...	...	...	...	...	...	...	...	...	...
He I	5876	...	...	...	...	...	...	2.7	3.7	...	...
[O I]	6300	...	...	206.2:	231.5:	16.9	19.0	32.1:	36.0:	...	...
[O I]	6363	...	...	60.0:	65.5:	3.0	3.3	...	...	...	...
[N II]	6548	...	...	153.8	154.7	87.3	87.8	64.9	65.3	100.3	100.9
Hα	6562	300.0	300.0	300.0	300.0	300.0	300.0	300.0	300.0	300.0	300.0
[N II]	6583	...	...	468.7	464.6	57.3	56.8	132.6	131.4	310.3	307.6
[S II]	6717	...	...	60.0	56.4	22.9	21.5	9.8	9.2	40.3	37.9
[S II]	6731	...	...	136.9	127.9	15.3	14.3	21.6	20.2	97.2	90.9
F(Hα), I(Hα)[c]		4.5	35.6	1.6	12.6	11.0	86.9	4.3	33.4	2.9	22.9
N_e (cm^{-3})		...		$\geq$10,000		$<$100		$\geq$10,000		$\geq$10,000	
$E(B-V)$[d]		0.9005[e]		0.9005[e]		0.9005[e]		0.8926		0.9005[e]	

		KNOT IDENTIFICATION[a]									
		D61		P2Diff.1[f]		P2Diff.2[f]		P2Diff.1 + 2[f]		SW of D9[g]	
LINE	λ	$F(\lambda)$	$I(\lambda)$	$F(\lambda)$	$I(\lambda)$	$F(\lambda)$	$I(\lambda)$	$F(\lambda)$	$I(\lambda)$	$F(\lambda)$	$I(\lambda)$
Hβ	4861	35.2:	94.3:	...	...	...	...	...	...	40.6	108.8
[O III]	4959	...	...	...	...	...	...	...	...	...	...
[O III]	5007	47.0:	113.8:	...	...	...	...	...	...	...	...
[N II]	5755	...	...	...	...	...	...	...	...	...	...
He I	5876	...	...	...	...	...	...	...	...	...	...
[O I]	6300	30.0:	33.7:	288.5	323.8	...	...	...	...	93.7	105.2
[O I]	6363	17.0:	18.5:	36.9	40.3	...	...	...	...	17.5:	19.1:
[N II]	6548	93.9	94.5	32.3:	32.5:	...	...	28.6:	28.8:	243.8	245.2
Hα	6562	300.0	300.0	300.0	300.0	300.0	300.0	300.0	300.0	300.0	300.0
[N II]	6583	260.9	258.6	49.6	49.2	...	...	39.5	39.2	750.0	743.4
[S II]	6717	30.0	28.2	...	...	...	...	...	...	143.8	135.1
[S II]	6731	67.8	63.4	...	...	...	...	...	...	287.5	268.8
F(Hα), I(Hα)[c]		2.3	18.2	2.6	20.6	1.6	12.6	4.4	34.8	4.8	37.9
N_e (cm^{-3})		$\geq$10,000		...		...		...		5400	
$E(B-V)$[d]		0.9005[e]		0.9005[e]		0.9005[e]		0.9005[e]		0.9005[e]	

TABLE 2—*Continued*

Line	λ	Knot Identification[a] D9, 10 F(λ)	D9, 10 I(λ)	D25 F(λ)	D25 I(λ)	D27 F(λ)	D27 I(λ)	D3[b] F(λ)	D3[b] (I(λ)	D9[b] F(λ)	D9[b] I(λ)
Hβ	4861	35.6	95.2	32.5	100.0	41.2	100.0	38.2	100.0	41.5	100.0
[O III]	4959	...	...	...	...	35.6	81.0	30.0	73.3	15.0:	34.0:
[O III]	5007	18.9:	45.8:	23.8	65.2	106.9	236.9	92.7	220.3	57.4	126.5
[N II]	5755	...	...	7.5	11.9	13.7	19.7	7.4	10.9	7.5	10.7
He I	5876	...	...	8.0	11.6	11.2	15.1	9.0	12.4	8.3	11.1
[O I]	6300	122.2	137.2	127.5	145.5	90.0	99.9	49.1	55.0	60.0	66.5
[O I]	6363	31.1	33.9	30.0	33.1	33.8	36.5	17.2	18.7	20.3	21.9
[N II]	6548	200.0	201.2	185.0	186.3	178.1	179.1	152.7	153.6	150.0	150.8
Hα	6562	300.0	300.0	300.0	300.0	300.0	300.0	300.0	300.0	300.0	300.0
[N II]	6583	600.0	594.7	575.0	569.2	543.8	539.4	463.6	459.6	458.8	455.2
[S II]	6717	97.8	91.9	87.5	81.5	60.0	56.7	106.4	100.1	71.5	67.6
[S II]	6731	211.1	197.3	180.0	166.7	125.6	118.2	169.1	158.3	141.2	132.9
F(Hα), I(Hα)[c]		27.0	213.4	12.0	127.0	160.0	1026.7	11.0	83.0	34.0	215.8
N_e (cm^{-3})		8000		5800		7000		2000		4900	
E(B−V)[d]		0.9005[e]		1.0277		0.8097		0.8804		0.8048	

Line	λ	Knot Identification[a] D18[b] F(λ)	D18[b] I(λ)	D47 + D48 F(λ)	D47 + D48 I(λ)
Hβ	4861	36.6	100.0	...	...
[O III]	4959	...	...	...	...
[O III]	5007	20.7	51.2	...	...
[N II]	5755	11.5	17.3	...	...
He I	5876	12.8	17.8	...	...
[O I]	6300	163.2	183.7	...	...
[O I]	6363	44.1	48.2	...	...
[N II]	6548	220.6	221.9	...	...
Hα	6562	300.0	300.0	300.0	300.0
[N II]	6583	661.8	655.8	...	...
[S II]	6717	141.2	132.5	...	...
[S II]	6731	273.5	255.3	...	...
F(Hα), I(Hα)[c]		6.8	56.0	4.7	37.2
N_e (cm^{-3})		4700		...	
E(B−V)[d]		0.9186		0.9005[e]	

[a] Knot identifications from D'Odorico *et al.* 1986.

[b] Knots D3, D9, and D18 were observed both with slit positions P1 and P4. Comparison gives an indication of the accuracy of various line measurements.

[c] F(Hα) and I(Hα) in units of 10^{-15} ergs cm^{-2} s^{-1}.

[d] Reddening correction assumes an intrinsic Hα:Hβ = 3.0.

[e] Mean extinction of bright filaments assumed.

[f] P2Diff.1 and P2Diff.2 are two portions of the northeast diffuse emission just northwest of knot D55. P2Diff.1 is closer to knot D55 and shows some weak [N II] emission.

[g] SW of D9 is a previously uncatalogued knot of emission about 45″ SW of knot D9 along the P3 slit position.

IV. DISCUSSION

We have sampled many of the bright radiative knots in the NW portion of Kepler's SNR and the spectra we have obtained generally confirm what has been seen previously. The densities derived from the observed [S II] lines are very high; using the formulation of Blair and Kirshner (1985), the densities in the radiative filaments range from 2000 cm^{-3} to more than 10,000 cm^{-3} as is indicated in Table 2. Comparison of the [S II] line ratios with those which have been calculated from shock models (Raymond 1979; Shull and McKee 1979; Hartigan, Raymond, and Hartmann 1987, hereafter HRH) indicate that preshock densities of order 100 cm^{-3} are required to produce the observed line ratios. On the other hand, the [S II] λ6731:Hα line ratios (~0.5 Hα) are typical for SNRs, which indicates that densities are not so high that [S II] λ6731 is collisionally de-excited, as occurs in HRH's models with preshock densities of 1000 cm^{-3}. There is in fact no correlation between the [S II] λ6731:Hα line ratio and the [S II] λλ6717:6731 line ratio, so it appears that the range of [S II] line strengths reflects differences in shock conditions or possibly abundances. [N II] emission is very strong in most of Kepler's radiative filaments, considerably stronger than is observed in most older SNRs, and stronger than is produced in models of radiative shocks when abundances are assumed cosmic. This is most likely due to an overabundance of nitrogen in many of the knots (see Bandiera 1987). The amount of the overabundance depends on the details of the shock model; typical ratios of [N II] λ6583 to Hα are 1.6 which implies overabundances of at least a factor of 2 based on HRH's models with equilibrium preionization. The high density and apparent overabundance of nitrogen clearly point to mass loss from the precursor star and imply that the radiative knots are circumstellar material that has been encountered by the main SNR shock. The optical emission arises behind secondary shocks

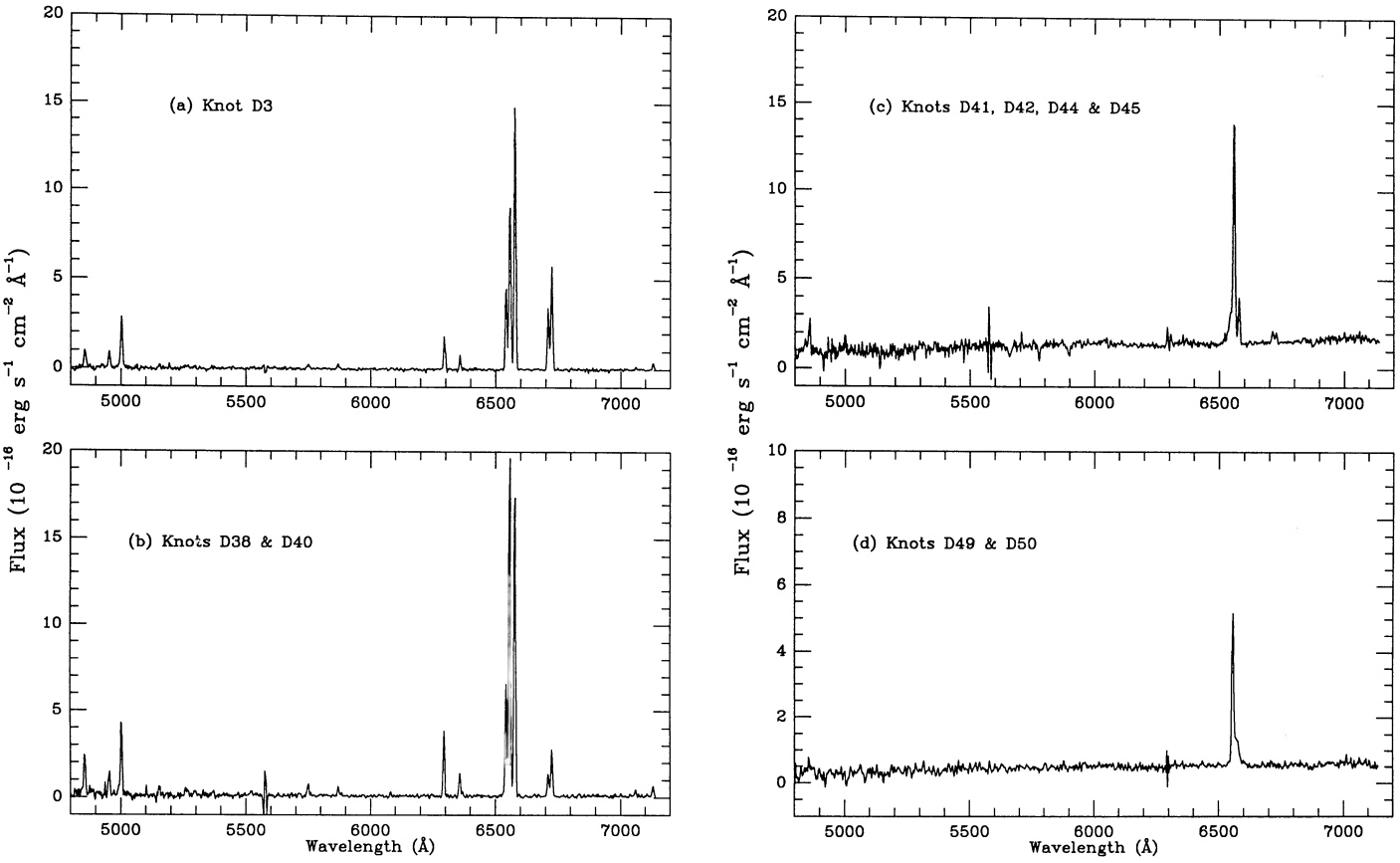

FIG. 7.—Selected one-dimensional low-dispersion spectra showing the variation of Balmer to forbidden line intensities for various knots. (*a*) Knot D3; (*b*) knots D38 and D40; (*c*) the D41, D42, D44, D45 complex; and (*d*) knots D49 and D50.

driven into these dense blobs of circumstellar material. Detailed comparison of our spectra with shock models is problematic given the limited number of lines in our spectral region and the difficulty of separating abundance effects from the physical conditions of individual shocks. The strength of [O III] λ5007 (50–230 relative to Hβ/100) suggests shock velocities of $\sim$100 km s^{-1} are typical (again assuming equilibrium preionization). (To accurately determine shock velocities, UV line strengths are needed; these will be difficult to obtain because of substantial absorption along the line of sight to Kepler's SNR.) The strength of [S II] and [N II] relative to Hα are correlated in our spectra which could reflect differences in the shock velocity or could indicate that the [S II] abundance is correlated with the [N II] abundance in various knots in Kepler's SNR.

The mean reddening $E(B-V)$ to Kepler's SNR is 0.9 ± 0.1; the error in our estimate is mainly systematic and is due to the 10% uncertainty in the relative calibration of the red and blue ends of the low-resolution spectra. This value is lower than the mean reddening of $E(B-V)$ of 1.1 given by Leibowitz and Danziger (1983) and somewhat higher than estimates of the foreground reddening $E(B-V) = 0.7 \pm 0.2$ based on photometry of the field stars (van den Bergh and Kamper 1977). We do find evidence of small variations of the reddening across the face of Kepler's SNR. These variations in $E(B-V)$, which can be seen in spectra extracted from single long-slit exposures, are typically of order 0.1. It is unlikely these variations can be attributed to instrumental effects. Similar variations in extinction from knot to knot were reported by Leibowitz and Danziger (1983). They also reported one knot in Kepler's SNR which appeared to have an Hα:Hβ ratio of $\sim$22 or $E(B-V)$ of 1.8. We have sampled many more knots than Leibowitz and Danziger (1983) and find no large variations in reddening, so this large variation is either spurious or at least a very uncommon phenomenon. Variations of order 0.1 in $E(B-V)$ correspond to differences in N_H of $\sim 7 \times 10^{20}$ cm^{-2}. It is not clear where these variations arise, but if they are due to clouds in the vicinity of Kepler's SNR, then assuming clouds of $\sim$5″ extent (= 0.1 pc) implies densities of order 1000 cm^{-3} for the clouds.

With the exception of a few relatively bright emission knots in the NE (e.g., D56, D61) most of the remaining emission we have sampled in Kepler's SNR has a different character from the bright radiative filaments in the NW. We have sampled the diffuse emission in the north (observed by Fesen *et al.* 1989, although at a different position angle) and find all of this emission to be dominated by Hα. No [S II] lines are seen in this diffuse component, and, if [N II] λ6584 is present, it is very weak ($\leq$10% of Hα peak intensity), especially given the probable overabundance of nitrogen in the shocked material. The Hα line in this northern diffuse emission seems to have a weak broad component at its base, confirming the result of Fesen *et al.* (1989). We conclude, as did they, that this is nonradiative shock emission; apparently the main SNR shock is encountering a lower density, more uniform component of the presupernova mass loss in the north (or perhaps the undisturbed ISM), and this component is at least partially neutral. The

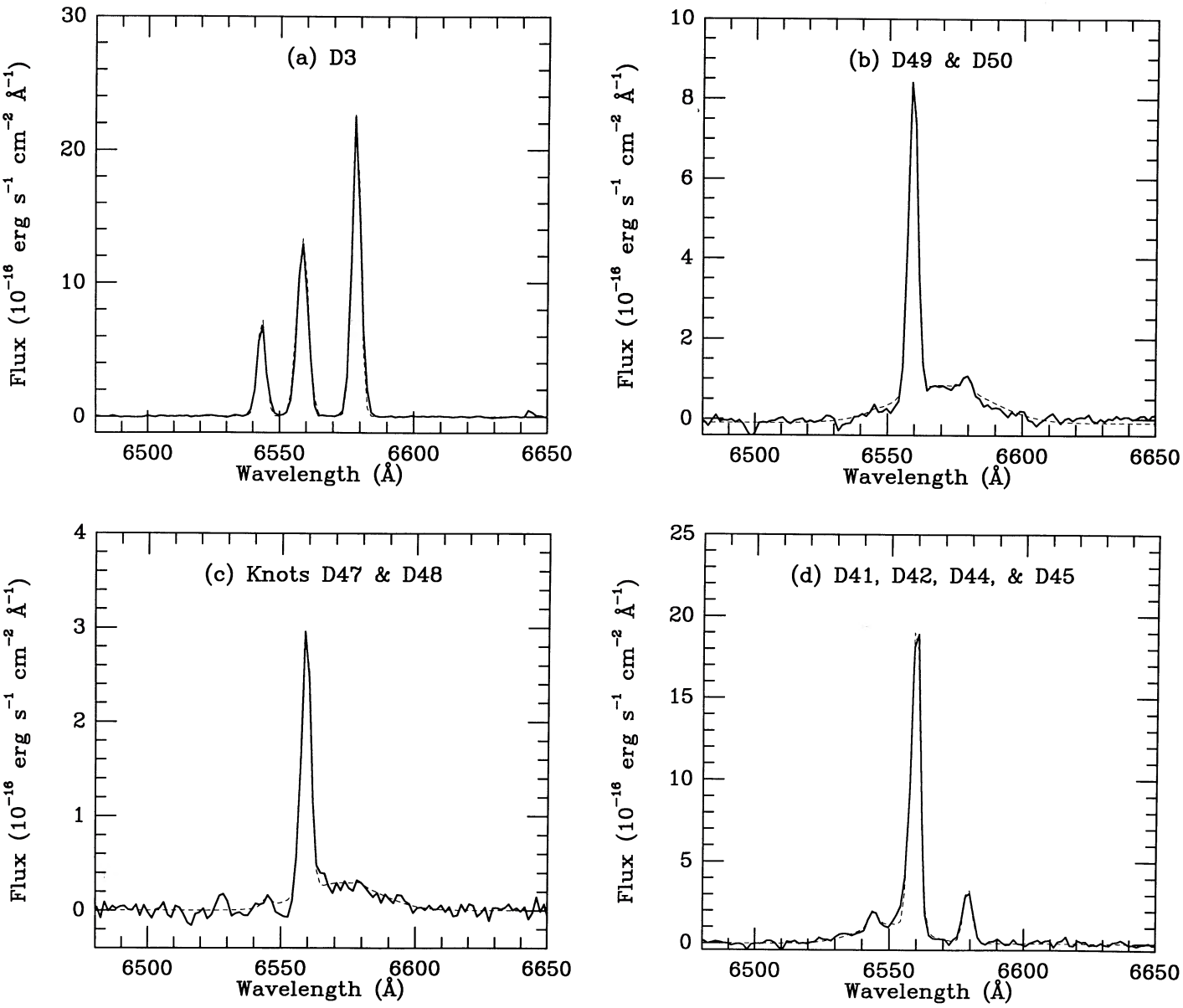

FIG. 8.—Multiple Gaussian component model fits to the Hα-[N II] regions of several filaments in Kepler's SNR from the 1989 August data: (*a*) the radiative filament D3; (*b*) the nonradiative filaments D49 and D50; (*c*) the nonradiative filaments D47 and D48; and (*d*) the transition filaments D41, D42, D44, and D45. The solid line is the data and the dashed line is the fit.

diffuse emission just west of the bright NW filaments visible in Figure 2*a* and at the NW end of the position 1 and position 4 spectra in Figure 6 apparently has the same character.

In addition to this diffuse emission, however, some of the knotty-type filaments also show nonradiative shock emission. The best example of this are knots D49 + D50, which have no detectable [S II] emission, and probably no [N II] emission adjacent to Hα, although some weak [N II] buried in the weak broad component of Hα cannot be entirely ruled out. This is the first time that Balmer-dominated emission has been detected in knotty-type structures.

Between the extremes of radiative and nonradiative filaments discussed above, it appears that some of the observed knots are in various stages of transition from nonradiative to radiative states. For example, knots such as D47 and D48 appear to have a weak but clearly resolved peak at the position of [N II] λ6584, even though the broad Hα component also appears present. A more extreme example may be the D41, D42, D44, D45 complex of knots (Fig. 8*c*): in this region, the broad component of Hα appears shifted slightly to the blue of the narrow component (presumably due to geometrical effects—see below) permitting the weak [N II] λ6584 line to be clearly seen. This position appears unique in our spectra of "transition" filaments in that it also has weak [S II] emission, with a ratio that indicates a much lower density than seen in the bright radiative filaments (see Table 2). Thus, this emission is not simply a superposition of a nonradiative and typical (for Kepler) radiative filament. Other transition filaments include knots D61 and D64, which have considerable [N II] and [S II] emission, but much weaker than observed in the bright radiative filaments (see D25, D27, etc.).

The width of the broad component provides information

TABLE 3

RESULTS OF MULTIPLE COMPONENT GAUSSIAN LINE PROFILE FITTING

Spectrum	Model[a]	Wavelength (Å)	Flux (ergs cm^{-2} s^{-1})	FWHM[b] (Å)	χ^2 / Degrees[c] of Freedom
NE Diffuse Emission[d]	I	6559.54	2.35E-15±7.43E-17	3.70±0.12	330.3 / 139
		6562.46±1.64	1.66E-15±1.95E-16	35.37±2.59	
	II	6559.54	2.72E-15±7.04E-17	4.12±0.12	264.9 / 138
		6544.8±0.96	2.02E-16±6.64E-17	3.67	
		6580.0±0.23	4.12E-16±4.46E-17	3.67	
	III	6559.54	2.46E-15±6.22E-17	3.84±0.12	217.5 / 135
		6544.55±0.97	1.57E-16±6.08E-17	3.67	
		6579.9±0.22	3.82E-16±4.22E-17	3.67	
		6559.42±2.18	1.09E-15±1.67E-16	35.46±3.79	
Knots D41,42,44,45[d]	I	6559.33	8.12E-15±2.62E-16	3.98±0.14	416.3 / 139
		6559.86±1.17	5.07E-15±0	41.23±0.14	
	II	6559.33	9.12E-15±2.28E-16	4.31±0.12	288.8 / 138
		6544.23±0.71	9.98E-16±2.09E-16	3.67	
		6579.1±0.21	1.38E-15±1.21E-16	3.67	
	III	6559.33	8.41E-15±1.98E-16	4.07±0.12	224.5 / 135
		6544.1±0.34	3.90E-16±9.83E-17	3.67	
		6579.1±0.07	1.35E-15±4.53E-17	3.67	
		6549.9±1.98	3.46E-15±1.41E-16	27.03±4.47	
Knots D49,50[d]	I	6559.26	3.37E-15±8.80E-17	3.93±0.12	142.9 / 139
		6570.86±0.26	4.02E-15±1.08E-16	39.16±0.68	
	II	6559.26	4.06E-15±1.24E-16	4.47±0.16	246.9 / 138
		6545.12±0.39	1.73E-16±1.08E-16	3.67	
		6579.0±0.23	5.89E-16±3.79E-17	3.67	
	III	6559.26	3.39E-15±8.86E-17	3.96±0.12	140.0 / 135
		6545.01±2.47	1.79E-17±3.94E-17	3.67	
		6579.4±0.45	1.32E-16±2.62E-17	3.67	
		6570.7±1.20	4.01E-15±1.75E-16	40.22±2.59	
Knots D47+48[d]	I	6559.17	1.18E-15±6.00E-17	4.00±0.24	220.4 / 139
		6571.12±2.28	1.21E-15±1.54E-16	36.12±4.38	
	II	6559.17	1.41E-15±6.99E-17	4.54±0.26	261.6 / 138
		6545.06±1.68	5.53E-17±4.14E-17	3.67	
		6578.99±1.28	1.47E-16±4.91E-17	3.67	
	III	6559.17	1.22E-15±6.1E-17	4.10±0.24	215.9 / 135
		6544.79±2.02	3.73E-17±3.78E-17	3.67	
		6579.3±4.23	1.27E-17±4.51E-17	3.67	
		6572.61±1.95	1.04E-15±1.37E-16	33.18±4.59	
Knot D3, Radiative Filament[d]	II	6558.57	7.24E-15±1.41E-16	5.11±0.12	1669.4 / 138
		6543.22±0.08	2.92E-15±9.65E-17	3.67	
		6578.52±0.02	9.05E-15±8.61E-17	3.67	
	III	6558.57	7.24E-15±1.42E-16	5.11±0.12	1663.0 / 135
		6543.22±0.08	2.92E-15±9.73E-17	3.67	
		6578.52±0.02	9.05E-15±8.69E-17	3.67	
		6568.78±74.88	9.40E-17±3.04E-16	70.64±96.90	
P2 Diffuse 2 Region in NE[e]	I	6559.87	1.49E-15±3.67E-17	8.12±0.24	76.0 / 53
		6557.89±3.14	1.23E-15±1.02E-16	76.41±7.39	
	II	6559.87	1.68E-15±4.39E-17	8.67±0.26	100.2 / 52
		6547.33±1.73	1.54E-16±4.29E-17	8.24	
		6580.52±1.84	1.13E-16±3.31E-17	8.24	
	III	6559.87	1.54E-15±3.67E-17	8.17±0.24	69.9 / 49
		6549.15±2.64	7.87E-17±3.69E-17	8.24	
		6580.87±3.10	3.29E-17±2.83E-17	8.24	
		6557.45±4.45	1.21E-15±1.09E-16	89.84±9.14	

Table 3, Continued

Spectrum	Model[a]	Wavelength (Å)	Flux (ergs cm^{-2} s^{-1})	FWHM[b] (Å)	χ^2 / Degrees[c] of Freedom
NW Diffuse Emission[e]	I	6559.06	4.60E-15±7.63E-17	8.36±0.16	184.9 / 53
		6560.35±3.10	2.01E-15±1.97E-16	50.91±5.30	
	II	6559.06	5.23E-15±7.04E-17	8.97±0.14	144.3 / 52
		6542.81±1.10	4.50E-16±7.22E-17	8.24	
		6579.68±0.74	5.24E-16±7.6E-17	8.24	
	III	6559.06	4.84E-15±6.97E-17	8.57±0.14	143.5 / 49
		6544.36	2.33E-16±7.16E-17	8.24	
		6579.91±0.93	3.28E-16±7.69E-17	8.24	
		6560.59±4.22	1.99E-15±2.18E-17	74.58±9.94	
SW of D9[e]	I	6557.47	4.99E-15±1.22E-16	8.71±0.26	106.2
		6542.86±0.16	3.96E-15±1.34E-16	8.24	
		6578.39±0.07	1.14E-14±1.49E-16	8.24	
	II	6557.47	4.91E-15±1.24E-16	8.71±0.26	104.7
		6542.87±0.17	3.91E-15±1.36E-16	8.24	
		6578.39±0.07	1.15E-14±1.52E-16	8.24	
		6568.19±60.56	1.77E-16±3.94E-16	69.96±27.55	

[a] Models: (I) Broad and narrow Hα without [N II] lines; (II) Narrow Hα and the [N II] lines with no broad component; (III) Broad and narrow Hα as well as the [N II] lines.
[b] Errors are formal 1 σ errors to the flux and the FWHM as produced by the line-fitting program.
[c] χ^2 errors obtained from rms fluctuations outside of the line region.
[d] From high-resolution data.
[e] From low-resolution data.

about the shock velocity in nonradiative filaments. It arises from a charge exchange reaction between slow neutrals and fast protons behind the shock. As the model calculations of CKR show, the width of the broad line depends upon assumptions made about the mechanism by which energy is shared between electrons and ions in the post-shock gas. For a given shock velocity, v_s, if electrons and ions equilibrate rapidly behind the shock ($T_i = T_e$) compared with the ionization time scale, then the ion temperature will be lower than if electrons and ions equilibrate on a Coulomb time scale ($T_i \gg T_e$). For a given shock velocity, the predicted width of the broad component, which is a measure of the postshock ion temperature, will be narrower if $T_i = T_e$ than if $T_i \gg T_e$. Based on the calculations carried out by CKR, we estimate the average shock velocity in Kepler to be 1550 km s^{-1} if $T_i = T_e$ and to be 2000 km s^{-1} if $T_i \gg T_e$. (Note: The shock velocity is 4/3 times the bulk velocity behind the shock.)

Similar information may also be contained in the ratio of flux in the broad and narrow Hα emission-line components, although, as emphasized recently by Smith and Kirshner (1989), the theory needed to interpret the broad-to-narrow line ratio is more difficult. Calculations have only been published for the situation in which $T_i \gg T_e$. (See Fig. 5 of Kirshner *et al.* 1987.) These calculations indicate that the ratio of the broad-to-narrow component should be a decreasing function of shock velocity, ranging from 3 at 1000 km s^{-1} to 0.6 at 2700 km s^{-1}. Our value for the broad-to-narrow line ratio 0.72 ± 0.37 corresponds to a shock velocity of 2200–3200 km s^{-1}, somewhat higher than the corresponding value estimated from the broad line width. However, most measured values of the broad-to-narrow line flux lie near 1 even when other estimates of the shock velocity indicate shock velocities of ≤1000 km s^{-1} (Raymond *et al.* 1983; Smith and Kirshner 1989; Long and Blair 1990). Hence, we regard the broad line width as a much more reliable estimator of the shock velocity in Kepler's and other SNRs.

The separation of broad and narrow components of emission provides information about the geometry of the shock. As might be anticipated, for the diffuse Hα emission on the NE rim, the broad and narrow components are centered on the same wavelength (within the errors), which is consistent with the shock being perpendicular to the line of sight. The broad component in knots D41, D42, D44, and D45, which are located near the projected center of the SNR, is blueshifted; presumably this complex of knots is on the near side of the SNR. In contrast, the broad Hα components in spectra extracted of knots D47 + D48 and of knots D49 + D50 appear to be redshifted; evidently these are on the far side. This suggests that the ridge of emission which crosses the center of Kepler's SNR at X-ray and radio wavelengths may not be a single physical entity.

The separation of the broad and narrow components also places lower limits on the shock velocity, since it represents the line-of-sight component of the bulk velocity of postshock gas with respect to the local ISM, which is ¾ of the shock velocity. For example, the difference in the centroid of the narrow and broad components of 13.4 Å or 610 km s^{-1} in the spectrum of knots D47 and D48 implies a minimum shock velocity of 815 km s^{-1}. This is much lower than our estimate of the shock velocity 1550–2000 km s^{-1} based on the width of the broad component. Evidently the shock at this position is moving at an angle 60–65 degrees with respect to the line of sight. Since knots D47 and D48 are located only 25″ from the X-ray/radio center of Kepler's SNR, a shock moving radially would be only about 14° out of the line of sight. Perhaps the shock is wrapping around a local density enhancement which creates the knots of emission we observe.

The absolute value of the Hα flux can be used to estimate the

density of the neutral component of the ISM being encountered by the shock, since each neutral H atom results in a certain number of Balmer photons. The expected flux can be parameterized as

$$\frac{dI}{d\Omega} = 6 \times 10^{-17} \frac{N_{\rm ph}}{0.2} n v_3 \frac{v}{v_{\parallel}} \text{ ergs cm}^{-2} \text{ s}^{-1} ,$$

where $N_{\rm ph}$ is the number of photons produced per neutral H atom, n is the preshock neutral density, v_3 is the shock velocity in units of 1000 km s^{-1} and $v/v_{\parallel}$ is the geometrical factor which defines the ratio of the total shock velocity to the line-of-sight velocity. Evidently, the best estimates can be derived for those shocks which are nearly face-on. For knots D47 and D48, we measure a dereddened Hα flux of $\sim 2.1 \times 10^{-15}$ ergs cm^{-2} s^{-1} arcsec^{-2}. For these knots, $v/v_{\parallel} = 1.8$–2.4, depending on whether the shock velocity is 1500 or 2000 km s^{-1}, and hence we require densities of 7–12 cm^{-3}, very similar to estimates of the density derived from X-ray measurements (5–10 cm^{-3}; White and Long 1983).

The shock velocity 1550–2000 km s^{-1} that we measure in the nonradiative filaments of Kepler's SNR is somewhat lower than measured in Tycho's SNR, in which measurements of the Balmer widths lead to shock velocity estimates of 1930–2670 km s^{-1} (Kirshner, Winkler, and Chevalier 1987). This may not be surprising, since X-ray and optical estimates of the density of the ambient material around Tycho's SNR are typically 0.3–0.9 cm^{-3} and thus Kepler's SNR should have decelerated more rapidly.

The proper motion of the Balmer-dominated filaments in Kepler's SNR is not known. When it is measured, it will be possible to use the shock velocity and the proper motion of the Balmer filaments to determine the distance to Kepler's SNR, as has been done for Tycho's SNR and SN 1006 (Kirshner, Winkler, and Chevalier 1987; Long, Blair, and van den Bergh 1988). The radiative filaments appear to expand at a rate of $\sim 0\farcs005$ yr^{-1} (van den Bergh and Kamper 1977), but these knots are unlikely to be moving at the shock velocity of the primary SNR shock. Based on VLA observations obtained over a four year period, Dickel *et al.* (1988) have recently measured the expansion rate of Kepler's SNR; they find that the size of the remnant has grown at a rate which is consistent with a mean expansion law of $R \propto t^{0.5}$, which corresponds to a proper-motion of $0\farcs13$ yr^{-1}. The northern half of the remnant appears to have expanded at a slower rate; there $R \propto t^{0.35}$, which implies $0\farcs09$ yr^{-1}. For a proper-motion of $0\farcs09$ yr^{-1} and a shock velocity of 1550 (2000) km s^{-1}, the implied distance to Kepler's SNR is 3.3 (2.5) kpc, which is lower than most recent estimates. If the distance is 5 kpc as was assumed earlier, then the nonradiative shocks we are observing must be moving at a speed which is less than the shock velocity of the SNR as a whole. This is possible if the emission we observe is from density enhancements which are slowing the shock locally. Since the local shock velocity varies as the inverse square root of the local density, a factor of 4 increase in the density would be required. If, on the other hand, the distance is really 2.9 ± 0.4 kpc, then, given the apparent magnitude of (-3.0 ± 0.5) for Kepler's SN (Bandiera 1987) and our measurement of the reddening ($A_V = 2.7 \pm 0.3$), we estimate the absolute magnitude of Kepler's SN to have been -18.0 ± 1.0, which supports the hypothesis than Kepler's SN was subluminous for a Type Ia. This lends some support to the idea that Kepler's SN may have been a Type Ib explosion.

The environment around Kepler's SNR is certainly more complex than around Tycho's SNR or SN 1006, the two other historical SNs in which nonradiative filaments have been found and studied in detail. Neither of these two SNRs show any evidence of the radiative filaments that are seen in Kepler's SNR. It seems likely that the difference in the morphology of the filaments in these two SNRs and Kepler's SNR is another manifestation of the complex circumstellar environment of Kepler's SNR.

V. SUMMARY

We have identified a large number of Balmer-dominated filaments in Kepler's SNR, including a system of filaments which are projected near the center of the SNR. Like other Balmer-dominated emissions, the Hα line shape is comprised of broad and narrow components which can be interpreted in terms of a fast shock traversing partially neutral material. The width of the broad component indicates shock velocities of 1550–2000 km s^{-1}, depending upon how energy is shared between particles immediately behind the shock. The diffuse and knotty appearance of many of these filaments is unusual and may reflect the fact that in Kepler's SNR the shock appears to be traversing circumstellar material lost from the supernova precursor. There also exist a number of filaments which have broad Hα lines but also show weak but detectable [N II] and, in some cases, [S II] emission. If the velocity of the primary shock from Kepler's SNR is comparable to the velocity indicated by the nonradiative filaments, then the distance to Kepler's SNR is ~ 3 kpc, somewhat lower than most previous estimates. Follow-up studies are required, however, to measure the proper-motion of the Balmer filaments and to completely elucidate the character of the nonradiative emission in Kepler's SNR.

It is a pleasure to thank the staff of the Las Campanas Observatory for their excellent support and assistance in the gathering of the data. We thank Fred Seward for providing the reprocessed X-ray data in advance of publication, and Jerry Kriss for making his Gaussian line-fitting software available to us. Bob Kirshner loaned us the interference filters used in the imaging portion of this program, and John Raymond provided insight into nonradiative shock processes. We gratefully acknowledge support from the JHU Center for Astrophysical Sciences for this research.

REFERENCES

Baade, W. 1943, *Ap. J.*, **97**, 119.
Bandiera, R. 1987, *Ap. J.*, **319**, 885.
Blair, W. P., and Kirshner, R. P. 1985, *Ap. J.*, **289**, 582.
Braun, R. 1987, *Astr. Ap.*, **171**, 233.
Chevalier, R. A., Kirshner, R. P., and Raymond, J. C. 1980, *Ap. J.*, **235**, 186 (CKR).
D'Odorico, S., Bandiera, R., Danziger, J., and Focardi, P. 1986, *A.J.*, **91**, 1382.
Dennefeld, M. 1982, *Astr. Ap.*, **112**, 215.
Dickel, J. R., Sault, R., Arendt, R. G., Matsui, Y., and Korista, K. T. 1988, *Ap. J.*, **330**, 254.
Dwek, E., Petre, R., Szymkowiak, A., and Rice, W. L. 1987, *Ap. J. (Letters)*, **320**, L27.
Fesen, R. A., Becker, R. H., Blair, W. P., and Long, K. S. 1989, *Ap. J. (Letters)*, **338**, L13.
Fesen, R. A., Blair, W. P., and Kirshner, R. P. 1982, *Ap. J.*, **262**, 171.
———. 1985, *Ap. J.*, **292**, 29.
Green, D. A. 1984, *M.N.R.A.S.*, **209**, 449.
Gunn, J. E., and Westphal, J. A. 1981, *Proc. SPIE*, **290**, 16.
Hartigan, P., Raymond, R., and Hartmann, L. 1987, *Ap. J.*, **316**, 323 (HRH).
Hughes, J. P., and Helfand, D. J. 1985, *Ap. J.*, **291**, 544.

Kirshner, R. P., Winkler, P. F., and Chevalier, R. A. 1987, *Ap. J. (Letters)*, **315**, L135.
Leibowitz, E. M., and Danziger, I. J. 1983, *M.N.R.A.S*, **204**, 273.
Long, K. S., and Blair, W. P. 1990, *Ap. J. (Letters)*, **358**, 13.
Long, K. S., Blair, W. P., and van den Bergh, S. 1988, *Ap. J.*, **333**, 749.
Matsui, Y., Long, K. S., Dickel, J. R., and Greisen, E. W. 1984, *Ap. J.*, **287**, 195.
Nomoto, K., Thielemann, F.-K., and Yokoi, K. 1984, *Ap. J.*, **286**, 644.
Raymond, J. C. 1979, *Ap. J. Suppl.*, **39**, 1.
Raymond, J. C., Blair, W. P., Fesen, R. A., and Gull, T. R. 1983, *Ap. J.*, **275**, 636.
Seaton, M. J. 1979, *M.N.R.A.S.*, **187**, 79P.
Seward, F. D. 1990, *Ap. J. Suppl.*, **73**, 781.
Shull, J. M., and McKee, C. F. 1979, *Ap. J.*, **227**, 121.
Smith, R. C., and Kirshner, R. P. 1989, *Bull. A.A.S.*, **21**, 1201.
Stone, R. P. S., and Baldwin, J. 1983, *M.N.R.A.S.*, **204**, 347.
Strom, R. G., 1988, *M.N.R.A.S.*, **230**, 331.
Tuohy, I. R., Dopita, M. A., Mathewson, D. S., Long, D. S., and Helfand, D. J. 1982, *Ap. J.*, **261**, 473.
van den Bergh, S. 1978, *Ap. J. Suppl.*, **38**, 119.
van den Bergh, S., and Kamper, K. W. 1977, *Ap. J.*, **218**, 617.
White, R. L., and Long, K. S. 1983, *Ap. J.*, **264**, 196.

WILLIAM P. BLAIR, KNOX S. LONG, and OLAF VANCURA: Center for Astrophysical Sciences, Johns Hopkins University, Charles & 34th Streets, Baltimore, MD 21218